

# Kinetic Friction and Atomistic Instabilities in Boundary-Lubricated Systems

Martin Aichele

*Institut Charles Sadron, 6 rue Boussingault, 67083 Strasbourg, France and  
Institut für Physik, Universität Mainz, 55099 Mainz, Germany*

Martin H. Müser

*Department of Applied Mathematics, University of Western Ontario, London, Ontario N6A 5B7, Canada  
(Dated: November 4, 2018)*

The contribution of sliding-induced, atomic-scale instabilities to the kinetic friction force is investigated by molecular dynamics. For this purpose, we derive a relationship between the kinetic friction force  $F_k$  and the non-equilibrium velocity distribution  $P(v)$  of the lubricant particles.  $P(v)$  typically shows exponential tails, which cannot be described in terms of an effective temperature. It is investigated which parameters control the existence of instabilities and how they affect  $P(v)$  and hence  $F_k$ . The effects of the interfaces' dimensionality, lubricant coverage, and internal degrees of freedom of lubricant particles on  $F_k$  are studied explicitly. Among other results we find that the kinetic friction between commensurate surfaces is much more susceptible to changes in (i) lubricant coverage, (ii) sliding velocity, and (iii) bond length of lubricant molecules than incommensurate surfaces.

PACS numbers: 46.55.+d — Tribology and mechanical contacts, 81.40.Pq — Friction, lubrication and wear in materials science

## I. INTRODUCTION

The every-day phenomenon friction is of great practical and economical importance, which is one of the motivations to improve our understanding of tribological processes [1, 2]. Friction between two solids differs from that between a solid and a fluid in that both static and kinetic friction appear finite, while the force between a solid and a fluid vanishes linearly with sliding velocity  $v_0$  at small  $v_0$ . Static friction  $F_s$  is the externally applied force necessary to initiate relative sliding motion between two solids, whereas kinetic friction  $F_k$  is the force needed to maintain the sliding motion. Phenomenological friction laws, which date back to da Vinci, Amontons, and Coulomb [3], often provide a good description on the macroscopic scale.

The microscopic origins of kinetic friction are still a matter of debate, even though it has long been recognized that kinetic friction must be due to dynamical instabilities [4, 5]. While there can be many different processes leading to instabilities, they all have in common that potential energy is converted abruptly into kinetic energy and ultimately lost as heat [6]. Although instabilities can occur on many different time and length scales, there has been an enhanced interest in identifying those that occur on atomic scales. This quest is not only motivated by the miniaturization of technical devices down to the nanometer scale, but also by the desire to better understand macroscopic friction. The understanding of single-asperity contacts is needed as basis for the full description of macroscopic friction, where the bulk-mediated coupling between contacts gives rise to additional effects.

Load-bearing, simple-asperity contacts are often in the order of microns. According to Hertzian contact me-

chanics and generalizations thereof, the pressure is rather constant in the contact with the exception of the areas close to the circumference, where pressure gradients are large. In the centre of the contact, most of the lubricant is squeezed out. One may assume that these boundary-lubricated areas often account for most of the energy dissipation when two solids are slid against each other, unless the solids are very compliant, in which case elastic instabilities may also contribute a significant amount to the net dissipation. If wear was the main source of friction, material would have to rub off from the surfaces much faster than observed experimentally [7]. Hydrodynamic lubrication would likewise result in values for friction orders of magnitude too small, if it were assumed to be the dominant dissipation process.

While the crucial role of surfactants for friction has certainly been recognized, relatively little attention has been paid to characterize dynamical instabilities in boundary lubricants. Most of the work on instabilities leading to friction is devoted to elastic processes, which are most simply described in the Prandtl-Tomlinson (PT) model [8, 9]. In the PT model, an atom is pulled over a substrate by a spring that moves at constant velocity  $v_0$ . If the spring stiffness is below a certain critical value, the atom's instantaneous velocity can exceed  $v_0$  by many orders of magnitude, see i.e. the discussion in Refs. 5, 6. This process results in non-vanishing  $F_k$  in the limit of zero  $v_0$  as long as thermal fluctuations are absent. There is, however, a crucial difference between instabilities in boundary lubricants and instabilities occurring in elastic manifolds that are modelled in terms of the PT model and related approaches such as the Frenkel-Kontorova model [10, 11]. In boundary lubricants, atoms are only weakly connected to each other and to the confining walls. As a consequence, bond breaking can occur, whereas in elastic models, bonds are treated as unbreak-

able. This seemingly subtle difference leads to different tribological behavior.

Two different avenues have been pursued in the recent past to study dynamics in boundary lubricants and its consequences for tribological properties. One is a minimalist approach, in which one single lubricant atom embedded between two shearing plates is considered [12, 13]. In the following, we will refer to this approach as the impurity limit. The other avenue incorporates a large ensemble of lubricant atoms [14, 15]. This approach can eventually include surface curvature and elastic deformation of the surfaces making it possible to study what effect the interplay of surface curvature and elastic deformations have on dry or boundary-lubricated friction [16, 17].

In this paper, we intend to analyze what features of simplistic models appear robust as the level of complexity in the description of the boundary lubricant is increased. Since kinetic friction is intimately connected with instabilities, we focus on the analysis of instabilities. In a precedent paper by one of us [18], it was found that the existence of instabilities in the impurity limit and as a consequence the friction-velocity relationship  $F_k(v_0)$  depends on the ‘details’ of the model. For instance, it was found that for 1D, commensurate interfaces, the sign of the first higher harmonic in the lubricant-wall potential determines: (a) whether or not the athermal kinetic friction remains finite in the zero-velocity limit, and (b) the exponent  $\beta$  that describes the finite-velocity corrections by

$$F_k(v) - F_k(0) \propto v_0^\beta. \quad (1)$$

Note that Eq. (1) changes its form when thermal noise is included into the treatment, i.e., it becomes linear at small velocities [18]. Depending on the ratio of the relevant energies and temperature, thermal effects may be negligible down to very small values of  $v_0$ .

While Ref. 18 is mainly focused on the impurity limit, we intend to extend the analysis in a systematic fashion to less idealized situations. For example, instead of simple spherical impurities, dimers and hexamers (6-mers) will be studied. Moreover direct interactions between lubricant particles will be included and the effects of increasing coverage will be discussed. The central assumption of our analysis is the existence of instabilities or ‘pops’ of certain degrees of freedom. A pop is a sudden, seemingly erratic motion of a particle (or a collective degree of freedom) characterized by a velocity much larger than the associated thermal velocity or the drift velocity of the atom. Pops heat the lubricant or alternatively they couple directly to the confining solid walls, i.e., by inducing phonons in the walls. They will eventually induce more dramatic effects such as generation of dislocations or abrade the surfaces. However, as argued above, these extreme processes are rare and hence presumably they are not responsible for the main part of the energy dissipation. This is the motivation to concentrate on the energy transfer to the phonon bath that is due to

elementary process in the lubricant. The underlying idea of the presented approach can be described as follows. Sliding-induced instabilities make the velocity probability distribution (PD) of the lubricant atoms deviate from the thermal equilibrium PD. This alters the balance of energy flow from and to the lubricant. The energy missing in this balance is provided by the external driving device.

In this paper, we will develop a simple kinetic theory that connects the energy dissipation with the velocity PD (Section II). After discussing the numerical techniques in Sec. III, we will apply the theory to models of boundary lubrication of various complexity. This will include both the impurity limit, which is discussed in Section IV, and more complex situations that include interaction between lubricant atoms (Section V). Section VI contains the conclusions.

## II. THEORY

### A. General Comments

The most fundamental assumption in this paper is that the interaction between the lubricant atom  $i$  and the confining wall can be decomposed into one conservative part  $V_w(\mathbf{r}_i)$  and one non-conservative term consisting of a damping force plus thermal noise.  $V_w(\mathbf{r}_i)$  depends only on the difference between the position  $\mathbf{r}_i$  and the positions of top wall  $\mathbf{r}_t$  and bottom wall  $\mathbf{r}_b$ . It can be written as

$$V_w(\mathbf{r}_i) = V_b(\mathbf{r}_i - \mathbf{r}_b) + V_t(\mathbf{r}_i - \mathbf{r}_t), \quad (2)$$

where depending on the model under consideration, the vectors  $\mathbf{r}$  can be one-, two-, or three-dimensional. Unless otherwise noted, the relative motion of the walls is imposed externally, i.e., by constant separation (or constant load) and constant relative velocity  $v_0 \mathbf{e}_x = (\dot{\mathbf{r}}_t - \dot{\mathbf{r}}_b)$  of the walls parallel to the sliding direction indicated by the unit vector  $\mathbf{e}_x$ . We assume the normal pressure variations to be small, which means that the coupling to each individual confining (crystalline) wall is periodic parallel to the interface, i.e., it is periodic in the  $xy$ -plane.

In the theoretical part of our treatment, we assume that the *non-conservative* force  $\mathbf{F}_{t,i}^{(\text{nc})}$  that a wall (here the top wall) exerts on the lubricant atom  $i$  consists of a simple, viscous damping term  $-\gamma_t(\dot{\mathbf{r}}_i - \dot{\mathbf{r}}_t)$  plus a random force  $\mathbf{\Gamma}_t(t)$ , thus

$$\mathbf{F}_{t,i}^{(\text{nc})} = -m_i \gamma_t (\dot{\mathbf{r}}_i - \dot{\mathbf{r}}_t) + \mathbf{\Gamma}_t(t), \quad (3)$$

where the random force  $\mathbf{\Gamma}(t)$  is chosen such that detailed balance is obeyed when the external stress is absent. Thus the usual  $\delta$  correlation of the random forces is assumed, namely [19]

$$\langle \mathbf{\Gamma}_t(t) \mathbf{\Gamma}_t(t') \rangle = 2D \gamma_t m_i k_B T \delta(t - t'), \quad (4)$$

where  $D$  is the physical dimension,  $k_B T$  is the thermal energy, and  $m_i$  the mass of lubricant atom  $i$ . Random forces plus damping term  $-m_i \gamma_t \mathbf{v}$  (we dub the sum *thermostat*) mimic the interactions with phonons and/or other excitations, which are not treated explicitly. Typically, the time scales associated with these excitations are short compared to the motion of a particle from one minimum to another, which justifies the assumption of  $\delta$  correlated random forces for our purposes. Of course, damping can and will be different normal and parallel to the interface. However, this detail does not have any significant consequences for the conclusions presented in this paper. Similarly, the explicit treatment of internal elastic deformations does not alter the major conclusions either.

We will now be concerned with the derivation of a formal equation for the friction force. In any steady-state of the system, the average force on the upper wall (or the lower wall) must be zero. If the time average was different from zero, the upper wall would be accelerated in contradiction to the steady-state assumption, as pointed out for instance, by Thompson and Robbins [15]. The net force on the upper wall consists of three contributions: The externally applied force  $\mathbf{F}_{\text{ext}}$ , the conservative force between lubricant and wall, and the non-conservative force done by the thermostat. The external force  $\mathbf{F}_{\text{ext}}$  does the work  $W_{\text{ext}}$  on the upper wall given by

$$W_{\text{ext}} = \int d\mathbf{r}_t \mathbf{F}_{\text{ext}}. \quad (5)$$

The kinetic friction force  $F_k$  follows from that expression as it equals the work done on the system by external forces divided by the distance moved.

Since the conservative potential is assumed to be periodic, it cannot do any net work on a steady-state system and we may not consider it in our energy balance. This implies that the work must be done on the thermostat. The power dissipated into the damping term is proportional to  $\gamma m (\dot{\mathbf{r}} - \dot{\mathbf{r}}_t)^2$ , however, parts of that contribution can be provided by the stochastic random force  $\mathbf{\Gamma}(t)$ . Hence, if we want to account only for the power  $P_{\text{ext}}$  that is dissipated into the damping term due to the *externally* applied force, we have to integrate over the velocity distribution  $P(v)$  but we have to subtract the contribution that is due to the random force. The latter contribution is very difficult to calculate. We assume that this heat flow from the random force into the impurity system is identical to that in thermal equilibrium, in which the equilibrium (Maxwell Boltzmann) distribution  $P_{\text{eq}}(v)$  applies. This yields

$$P_{\text{ext}} = N_{\text{fl}} \gamma m \int_0^\infty v^2 \{P(v) - P_{\text{eq}}(v)\} dv, \quad (6)$$

where  $N_{\text{fl}}$  is the number of lubricant atoms,  $v$  is the velocity of a particle relative to the center-of-mass motion of the upper wall. The net external driving force (or in other words the kinetic friction force  $F_k$ ) can now be associated with

$$F_k = P_{\text{ext}}/v_0. \quad (7)$$

We want to emphasize that Eqs. (5) through (7) allow one to calculate friction forces under more general conditions than those of our particular model, for instance, if the thermostat only acts on the atoms in the outermost layers of the walls as e.g. employed in Ref. [20]. The approach can also be extended in a straightforward manner if generalized forms of the thermostat are employed such as in dissipative particle dynamics [21] or if the thermostat is based on a Mori Zwanzig formalism [22, 23]. The main limitation of Eq. (6) in the present context is that effects due to heating of the walls are not included. Again, a minor modification would allow one to include heating of the walls into the presented framework as well. However, as we will mainly focus on small velocities, the mentioned effects will be small and shall be neglected in the following.

Note that an alternative way of determining the friction force in the steady state is to time average the conservative plus the non-conservative force that the upper wall exerts on the lubricant. The observation that the work done by the conservative force is essentially zero does not imply that its time-average must be zero. A formal derivation of the conclusions from this section is given in the appendix.

## B. Effect of Instabilities

As discussed in the introduction, the externally imposed relative motion of the confining walls may induce sudden, dynamic instabilities or ‘pops’ during which the particles’ velocities greatly exceed both their thermal velocities and the relative sliding velocity  $v_0$  of the walls. This means that at a time  $t + \delta t$  the atom does not find a stable position in the  $\mathcal{O}(v_0 \delta t)$  vicinity of the old stable position at time  $t$ . The continuous trajectory ends at  $t$  and the particle has to move to the next mechanically stable position to resume its path. The particle will then pop into the next local potential minimum and for low sliding velocities, its peak velocity  $v_{\text{peak}}$  will be solely determined by the energy landscape and consequently  $\lim_{v_0 \rightarrow 0^+} v_{\text{peak}}/v_0$  diverges. Its kinetic energy will be dissipated (e.g. by phonons) and lead to friction. This process will lead to a deviation of the velocity distribution  $P(v)$  from the thermal equilibrium distribution  $P_{\text{eq}}(v)$  valid for  $v_0 = 0$ . Fig. 1 shows such instabilities for a model system that is described in detail in Sect. III.

The velocity distribution  $P(v)$  and hence the friction force  $F_k$  can be calculated in principle, once the precise form of the lubricant’s interaction is known. Risken’s book on the Fokker-Planck equation [19] gives an excellent overview of methods that allow one to treat models like ours, namely externally-driven systems that are mainly deterministic but also contain a certain degree of thermal noise. An analytical approach remains difficult in our case, due to the potential’s complex time dependence. Therefore a different, phenomenological approach will be pursued.

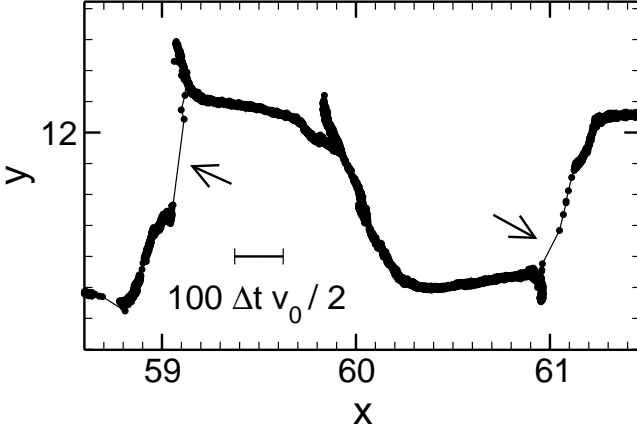


FIG. 1: Trajectory of a lubricant impurity in the  $xy$ -plane tagged between two incommensurate surfaces (at large load and small temperature). The relative velocities of the walls is  $v_0 = 10^{-3}$ . The positions are plotted every  $\Delta t = 0.5$ . The bar denotes 100 times the average drift distance per time interval  $\Delta t$ . The arrows indicate dynamical instabilities.

An instability will invoke a trajectory during which potential energy is abruptly converted into kinetic energy. The kinetic energy will then be dissipated into the thermostat, i.e., the phonon bath of the confining walls. After some time, which depends on the coupling strength to the thermostat, the Maxwell-Boltzmann probability distribution (PD) will be resumed, provided no new instability has been invoked in the meantime. An instability will thus create a typical velocity PD that will show up as a *tail* in the Maxwell-Boltzmann PD. Unless the two confining walls are identical and perfectly aligned (thus commensurate), there is a class of instabilities in which the energy lost during the ‘pop’ shows a broad distribution, see also Ref. 24. Every pop, characterized for instance by the energy dissipated, will contribute to  $P(v)$  in its own way. We assume that the net sum  $P_{\text{tail}}$  of all these individual tails shows exponential dependence on velocity, thus

$$P_{\text{tail}} \propto \exp(-B |\mathbf{v} - \bar{\mathbf{v}}|), \quad (8)$$

where  $\bar{\mathbf{v}}$  is the average velocity of the impurity under consideration, typically  $\bar{\mathbf{v}} = v_0 \mathbf{e}_x / 2$ , and  $B$  is a constant. The motivation for this particular choice of  $P_{\text{tail}}$  partly stems from Jaynes’ principle of information theory [25]. From it follows that the most likely normalized PD on  $[0, \infty)$  with given mean value about which we do not have more knowledge is the exponential distribution [26], thus an exponential ansatz for  $P_{\text{tail}}$  is plausible. Further restraints lead to deviations from an exponential form. While these considerations are heuristic, our choice of  $P_{\text{tail}}$  happens to be a quite accurate description for the velocity PDs of impurities between 2D, incommensurate surfaces. This will be demonstrated later in the result section.

At small sliding velocity  $v_0$ , the statistical weight of the tails must increase linearly with velocity. Hence, the

normalized PD function for the  $x$  component is given by

$$P(v_x) = \sqrt{\frac{m}{2\pi k_B T}} \left(1 - \frac{2A'v_0}{B'}\right) e^{-m(v_x - \bar{v}_x)^2 / 2k_B T} + A'v_0 e^{-B'|\mathbf{v}_x - \bar{\mathbf{v}}_x|}. \quad (9)$$

Here  $A'$ , and  $B'$  are phenomenological parameters that can (and will) depend on the externally applied load  $L$  that an impurity has to counterbalance, damping  $\gamma$ , and other parameters. However, they should depend only weakly on temperature  $T$  and sliding velocity  $v_0$  at small  $T$  and small values of  $v_0$ . This is because  $A'v_0$  is a measure for the rate of the fast processes (which should be proportional to  $v_0$  at small  $v_0$ ), while  $B'$  characterizes the instability related velocity PD. For 1D systems  $B' = B$ , the projection of a 2D exponential PD on one axis however leads to different  $A'$  and  $B'$  [27]. Inserting Eq. (9) into Eqs. (6) and (7) and integrating over  $v_x$  yields the following friction force per impurity atom  $F_k/N_{\text{fl}}$ :

$$\frac{1}{N_{\text{fl}}} F_k = 4\gamma m \frac{A'}{B'^3} - 2\gamma \frac{A'}{B'} k_B T, \quad (10)$$

from which the friction coefficient  $\mu_k = F_k/(N_{\text{wall}}L)$  follows. (Here,  $L$  is the average load carried per atom belonging to an outermost wall atom, thus  $F_k$  and  $N_{\text{wall}}L$  represent respectively the net friction force and the net load.) Of course, Eq. (10) can only be valid as long as Eqs. (8) and (9) give an accurate description of the non-equilibrium velocity PD and provided that the heat flow from the thermostat into the impurities is close to the thermal equilibrium heat flow. At extremely small  $v_0$ , two arguments show that the assumption of exponential tails cannot persist. First, the energy  $\Delta E_{\text{diss}}$  that is dissipated during a pop has an upper bound, which in turn implies an upper bound for the peak velocity. Second, close to equilibrium, thermal noise is sufficient to invoke (multiple) barrier crossing and recrossing. The ratio of sliding and noise-induced instabilities becomes small, which in turn makes the non-equilibrium corrections be less significant.

Eq. (10) is based on the one-dimensional distribution functions  $P(v_x)$ . For two-dimensional interfaces and boundary lubricants, the relevant PD is  $P(v_{\parallel})$  with  $v_{\parallel} = \sqrt{v_x^2 + v_y^2}$ . We want to note in passing that accumulating the histogram  $P(v_{\parallel})$  contains the same required information as  $P(v_x, v_y)$ , however, it requires less data storage. This is why for 2-dimensional boundary lubricants, we monitor  $P(v_{\parallel})$  instead of  $P(v_x, v_y)$ . Assuming rotational symmetry, Eq. (9) can be replaced with

$$P(v_{\parallel}) = 2\pi v_{\parallel} A v_0 e^{-B v_{\parallel}} + \left(1 - \frac{2\pi A v_0}{B^2}\right) P_{\text{eq}}(v_{\parallel}), \quad (11)$$

where  $A$  and  $B$  are phenomenological coefficients with similar meanings as their counterparts  $A'$  and  $B'$  in the one-dimensional description.

Inserting Eq.(11) into Eq. (6) yields:

$$\frac{1}{N_{\text{fl}}} F_k = 12\pi\gamma m \frac{A}{B^4} - 4\pi\gamma \frac{A}{B^2} k_B T \quad (12)$$

The parameters  $A$  and  $B$  will be obtained by fitting the PDs accumulated during MD simulations. If such fits turn out to be good approximations (and they do for incommensurate surfaces), then one has to ask into question descriptions of frictional interfaces that are based on local effective temperature (and local pressure). Local effective temperatures would imply Gaussian rather than exponential velocity tails. As we will argue later, this difference might matter with regard to chemical reactivity in a frictional interface.

Of course, the fits will never be perfect, and one has to address the question whether one can obtain information experimentally on  $A$  and  $B$ , i.e., by measuring  $F_k$  and the average kinetic energy of the lubricant atoms. We will therefore compare the values of  $F_k$  that are calculated directly (by averaging the force on the top wall) with those that are obtained indirectly with Eq. 12 after  $A$  and  $B$  are obtained through fits.

### III. MAIN MODEL AND METHODS

In this paper, we analyze the trajectories of atoms and molecules embedded between two walls in relative sliding motion by means of molecular dynamics. Different models with varying degree of complexity are investigated ranging from rather simple, 1-dimensional impurity models to 3-dimensional systems, in which the interaction between the lubricant particles are taken into account. In the latter case, lubricant particles are not only simple atoms but may also represent short polymers. Here, we will only describe the methods relevant to the full 3-dimensional simulations, as all other cases only require 'dumbed-down' versions of that method or small alterations thereof, such as suppressing the interaction between lubricant atoms.

In our model, lubricant atoms interact with each other and with wall atoms via a truncated Lennard Jones potential

$$V_{\text{LJ}}(r) = \begin{cases} 4\epsilon \left[ (\sigma/r)^{12} - (\sigma/r)^6 \right] + C, & r < r_c \\ 0, & r \geq r_c \end{cases}, \quad (13)$$

where  $r$  is the distance between two atoms.  $\epsilon$  defines the energy scale and  $\sigma$  the length scale of the system. Both quantities are set to unity. A constant value  $C$  is added to the potential for inter-atomic distances smaller than the cut-off radius  $r_c$ , which assures the continuity of the potential.  $r_c$  was chosen as the minimum of the LJ potential,  $r_c = r_{\text{min}} = 2^{1/6}$ , unless otherwise noted. This choice corresponds to a purely repulsive interaction and can be justified by the observation that at large pressures the essential behavior is caused by the repulsion of the particles. The main effect of including the attractive LJ

contribution in the present context would be to add an adhesive pressure. Throughout the paper quantities are measured using LJ units, such as time in units of  $t_{\text{LJ}} = (m\sigma^2/\epsilon)^{1/2}$  and forces in units of  $\epsilon/\sigma$ . Atomic masses  $m$  are also set to unity.

Both top and bottom wall lie in the  $xy$  plane and consist of  $N_{\text{wall}}$  discrete atoms arranged in the hexagonal (1,1,1) plane geometry of an fcc crystal. The nearest neighbor spacing  $d_{\text{nn}}$  in the walls is  $1.20914\sigma$  unless noted otherwise. This choice of  $d_{\text{nn}}$  does not match with other length scales in the system. Moreover, the relatively large value for  $d_{\text{nn}}$  enhances the effect of surface corrugation. In most simulations presented here, the normal load is kept constant. The load  $L$  will be stated in terms of normal load per atom in the upper wall, hence a unity normal load corresponds to a pressure of about 0.79 in reduced quantities.

Commensurate wall geometries were realized by orienting the two walls in parallel, whereas incommensurability was achieved by rotating the upper solid surface by  $90^\circ$ . The use of periodic boundary conditions in the wall plane required a slight distortion of the perfect hexagonal geometry in order to obtain two quadratic walls. Therefore, walls were not perfectly incommensurate anymore, but quasi-incommensurate (as every setup realized with finite number precision, strictly speaking). A wall unit cell consists of two atoms, at positions  $(0, 0)$  and  $(d_{\text{nn}}/2, \sqrt{3}d_{\text{nn}}/2)$ . By choosing the ratio of the wall unit cells in  $\hat{x}$  and  $\hat{y}$  close to the ideal value  $\sqrt{3}$  this distortion was minimized. We do not use other relative wall rotations in the full 3-dimensional simulations, as it was found in the study of similar models that the influence of the rotation angle is weak if it exceeds  $\approx 5^\circ$  [28]. We note that when two solids in an experiment come in contact they will most likely be incommensurate, as it would take utmost care to have two identical defect-free crystals and orient them perfectly. As detailed calculations show, elastic deformations do not generally alter this argument provided the solids are treated as 3-dimensional objects [6, 29].

While our analysis is focused on simple fluids, we include some work on small chain molecules in order to study aspects of molecular lubricants. To this end, we used a well established bead-spring model proposed by Kremer and Grest [30], which models individual monomers as LJ particles while chain connectivity is ensured by a FENE (finitely extensible nonlinear elastic) potential given by

$$V_{\text{FENE}} = -\frac{1}{2}k_{\text{ch}}R_{\text{ch}}^2 \ln [1 - (r/R_{\text{ch}})^2], \quad (14)$$

with  $R_{\text{ch}} = 1.5\sigma$  and  $k_{\text{ch}} = 30\epsilon/\sigma^2$  [30]. Typical values for hydrocarbons are  $\epsilon \approx 30\text{meV}$ ,  $\sigma \approx 0.5\text{nm}$ , resulting in a typical time scale of  $t_{\text{LJ}} \approx 3\text{ps}$  [30].

Simulations were done using a fifth order Gear-predictor corrector algorithm (see e.g. [31]) with an integration step of  $dt = 0.005$ . To maintain constant temperature, a stochastic Langevin thermostat was em-

played [32]. It consists of ideal white noise random forces and damping forces acting on all thermostatted particles, which obey the fluctuation-dissipation theorem [32]. A damping constant  $\gamma = 0.5$  was used in all simulations. In the presence of instabilities, the precise choice of  $\gamma$  is usually quite irrelevant for friction forces at small velocities [33], i.e., for the choice  $\gamma_b = 0.5$  and  $\gamma_t = 0$  we may expect similar friction forces as for the perhaps more natural choice of  $\gamma_b = \gamma_t = 0.25$ , if  $v_0$  is sufficiently small. However, in either case, one must ensure that the random forces satisfy the fluctuation dissipation theorem.

#### IV. IMPURITY LIMIT

##### A. 1D model systems

Here, we want to discuss and extend those results from Ref. 18 that are relevant to this study. In Ref. 18, the following potential  $V_t$  for the interaction between the impurity and the (one-dimensional) top wall was employed

$$V_t = V_{t,0} \cos(2\pi(x - x_t)/b_t) + V_{t,1} \cos(4\pi(x - x_t)/b_t), \quad (15)$$

$b_t$  being the lattice constant of the upper wall. A similar impurity-wall coupling is used to describe the interaction for the bottom wall, however, the indices  $t$  (for top) have to be replaced with  $b$  (for bottom). This is a generalization of the interactions suggested in Refs. 12 and 13 in that a non-zero first higher harmonic  $V_{t,1}$  is considered in Ref. [18]. Moreover, the lattice constant of the bottom wall  $b_b$  is allowed to differ from that of the top wall  $b_t$ . We note in passing that Refs. 12 and 13 were concerned with the interplay between external driving and embedded system, while Ref. 18 focused on the constant-velocity friction in such systems.

In Ref. 18, it was found that the behavior of the steady-state, low-velocity kinetic friction is surprisingly rich. For instance, athermal, zero-velocity friction turned out to vanish for  $V_{t,1} = V_{b,1} \leq 0$ . In that case, athermal, small-velocity friction can be described as a powerlaw  $F_k \propto v_0^\beta$  with a non-universal exponent  $0 < \beta < 1$ . For  $V_{t,1} = V_{b,1} > 0$ ,  $F_k$  remains finite as  $v_0$  approached zero. The case of  $V_{t,1} = V_{b,1} = 0$  is particularly intriguing, as the minima move at constant velocity  $v_0/2$ , then at some points in time (when there is perfect destructive interference of  $V_t$  and  $V_b$ ), the location of the potential energy minima make a ‘phase jump’ by a distance  $b_t/2$ . This phase jump, however, does not result in significant energy dissipation, as the location from where the impurity stems and the location where the impurity ends up are symmetrically equivalent.

For incommensurate walls ( $b_t \neq b_b$ ), the behavior is even richer. If the first higher harmonic is not included, one wall exerts a maximum force on the impurity and drags the impurity along. As a consequence,  $F_k$  is linear in  $v_0$ , which we call Stokes friction. For one certain

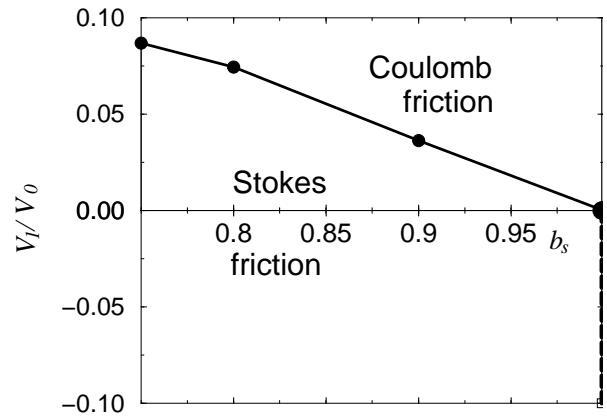


FIG. 2: Kinetic friction diagram for the impurity limit in 1 dimension.  $V_1/V_0$  is the ratio of first-higher harmonic and fundamental harmonic in the lubricant-wall interaction.  $b_s = b_b/b_t$  is the ratio of the two lattice constants. On the solid line and the dashed line, athermal kinetic friction is described by a power law  $F_k(v_0) \propto v_0^\beta$  with a non-universal exponent  $0 < \beta < 1$ . In the Stokes regime below the solid line,  $F_k \propto v_0$ . In the Coulomb regime above the solid line,  $F_k(v_0 \rightarrow 0)$  remains finite. The solid line is an interpolation between the circles, which reflect points in the parameter space that have been explicitly investigated.

value of the first higher harmonic  $V_{t,1}^*$  (at a fixed ratio  $b_s = b_b/b_t$ ),  $F_k$  can best be described as a power law in the limit of small  $v_0$ . For  $V_{t,1} > V_{t,1}^*$ ,  $F_k$  remains finite in the limit  $v \rightarrow 0$ , again provided thermal fluctuations are absent. Fig. 2 shows a friction diagram for the 1D, impurity-lubricant model. In order to yield a more complete picture than that given in Ref. [18], additional calculations have been carried out, in order to determine  $V_{t,1}^*$  for different values of  $b_s = b_b/b_t$ .

For a more detailed discussion of the effect of thermal fluctuations and the occurrence of a Stokes friction regime in one dimension and its potential applications, we refer the reader to Ref. 18.

##### B. 2D model systems

###### 1. Model details

We now allow the lubricant atoms to move within the  $xy$ -plane, but motion normal to the interface in  $z$  direction is still neglected. Eq. (15) must then be replaced with a new model potential. As in other studies, we consider the symmetry of the confining walls to be triangular, i.e., (111) surfaces of an fcc crystal, for which the potential  $V_t$  between top wall and an impurity can be written as:

$$V_t(\mathbf{x}, z) = \sum_{\mathbf{g}} \tilde{V}_t(\mathbf{g}, z) \exp\{i\mathbf{g}(\mathbf{x} - \mathbf{x}_t)\}. \quad (16)$$

In Eq. (16), the sum goes over all *two-dimensional* reciprocal lattice vectors of the trigonal lattice  $\mathbf{g}$ ,  $\mathbf{x}$  is the

position of the lubricant particle in the  $xy$  plane and  $\mathbf{x}_t$  the in-plane position of the (top) wall.  $z$  denotes the (fixed) distance between (top) wall and impurity.

The Fourier coefficients  $\tilde{V}_t(\mathbf{g}, z)$  between chemically non-bonding species often decay exponentially with  $|\mathbf{g}|$  and increasing distance from the surface  $z$ , thus  $\tilde{V}_t(\mathbf{g}, z)$  can be written as

$$\tilde{V}_t(\mathbf{g}, z) = \tilde{V}_t(\mathbf{g}, 0) \exp\{-\alpha|\mathbf{g}|z\}, \quad (17)$$

where both parameters  $V_t(\mathbf{g}, 0)$  and  $\alpha$  depend on the chemical nature of impurity atom and confining wall. Potentials of this form are known as Steele potentials [34]. They have proven to describe the potential energy landscape of atoms on crystalline surfaces reasonably well [35]. The fundamental harmonic in this potential is related to the smallest non-zero lattice vector  $\mathbf{g} = (2\pi/\sqrt{3}, 0)$  and its five symmetrically equivalent counterparts, which are obtained by rotating  $\mathbf{g}$  successively by  $60^\circ$ . (Note that the distance between 'atoms' in the walls is set to unity, which differs from the choice for the full 3D simulation model, see Sect. III.) First higher harmonics are related to reciprocal lattice vectors that are the sum of a suitable pair of two different fundamental  $\mathbf{g}$ 's and so on. The fundamental harmonic will be dominant at small loads, however, as the external pressure increases (which makes  $z$  decrease), the *relative* importance of higher harmonics will increase due to Eq. (17). The coupling between impurities and bottom wall is similar to that between impurities and top wall, however, the reciprocal vectors  $\mathbf{g}$  are rotated an angle  $\theta$  with respect to the top wall's  $\mathbf{g}$ 's. Two walls are called commensurate if  $\theta$  is an integer multiple of  $60^\circ$ . An equivalent 2D model without higher harmonics, was used recently by Daly et al. [24] for a study similar to that presented here.

In the following, we will be concerned with an analysis of mechanically stable position for the impurity atoms and their motion as the walls slide against each other. The goal is to identify situations, where the trajectory of a mechanically stable position suddenly disappears, which would lead to a dynamical instability. Such an analysis was given for 1D lubricants in Ref. [18], see Fig. 1 in that paper, and also in Ref. [24] for 2D systems. For our analysis, the bottom wall's lateral position  $\mathbf{x}_b$  is kept fixed, while  $\mathbf{x}_t$  is moved in small constant increments  $d\mathbf{x}$  with  $|d\mathbf{x}| \equiv dx = 10^{-5}$  to  $10^{-2}$ . After identifying an initial relative minimum in the impurity wall potential  $V_{i,w} = V_b + V_t$ , a steepest descent algorithm (we used the Mathematica function FindMinimum[] [36]) searches for the closest minimum in  $V_{i,w}$  in the vicinity of the previous one. If the distance  $\Delta d$  between the location of the new and the old minimum is greater than  $\Delta d = 0.1$ , we say that we identify a *pop*. While this choice of  $\Delta d$  is somewhat arbitrary, we ensured that our conclusions remained unaltered when  $\Delta d$  was varied in reasonable bounds and  $dx$  was further decreased. Since both methods employed in this study (simulations and steepest descent) are exact and identical within controllable errors, their results

mutually agree within these margins.

## 2. Commensurate Walls

Impurity atoms between commensurate walls only have a finite number of non-equivalent minima in their potential energy landscape. Once a minimum is identified, symmetrically equivalent minima will exist at periodically repeated positions that follow from the lattice of the confining walls. Various mechanically stable 'stacking' geometries can be envisioned for our walls of trigonal symmetry, for instance hexagonal close packed (hcp) and face cubic centered (fcc) type configurations best characterized as respectively *ABA* and *ABC* layering structures. The boundary lubricant reflects the middle layer. While it does not correspond to an ideally crystalline layer, the probability for a lubricant atom to sit at a certain position would be indeed periodic, i.e. it would have a maximum in every single *B* position.

As the two walls are slid with respect to each other, the situation is akin of the relative sliding of two commensurate, *one-dimensional* surfaces [18]. The 'trajectories' of mechanically stable positions bifurcate and recombine at certain relative, lateral displacements of the two solids, see Fig. 1a in Ref. [18]. This scenario invokes so-called *continuous* instabilities. The peak velocities during continuous instabilities tends to zero as  $v_0$  tends to zero, however, this does not happen linearly. This will ultimately lead to the following behavior if the walls are slid parallel to a symmetry axis and the top wall is allowed to move freely in transverse direction: After every half lattice constant moved, the system will convert from an fcc type structure to an hcp type structure or vice versa. This behavior is also found in our 3D default system (see Fig. 3), in which impurities interact with wall atoms through Lennard Jones potentials rather than through Steele potentials. The situation changes, when the top wall is not allowed to move in the transverse direction, which was the choice in Ref. 24. In that case, particles will occupy positions with high potential energy, which leads to instabilities. In this study, however, we focus on the case of zero transverse force.

As the mechanically stable positions of the embedded impurities show no discontinuities, the kinetic friction force will tend to zero at small  $v_0$  even if thermal fluctuations are absent. From the comparison to the 1D model systems, one would expect a powerlaw behavior as in Eq. (1) with  $F_k(0) = 0$ . This behavior does not depend on the sliding direction. It is also observed for ratios of  $V_t(\mathbf{g}, z)/V_b(\mathbf{g}, z)$  different from unity.

A central issue in the present paper is the question how robust the property of the simple impurity model is as more complexity is added to the model. In the present case, one may argue that lubricant atoms would be able to move in a correlated fashion up to a coverage of one monolayer. Above this coverage, the impurity model breaks down for obvious reasons.

### 3. Incommensurate Walls

Impurity atoms between incommensurate walls have an infinite number of inequivalent minima in their potential energy landscape for a given relative wall displacement. This means that at a given moment in time, it is impossible to find two different positions where the value of the potential and all its derivatives are identical. Yet, the number of inequivalent trajectories of (meta)stable positions can be small, because in most cases, they will all be identical up to temporal shifts when the walls are in relative sliding motion. See also the discussion of the dynamics of the incommensurate Prandtl-Tomlinson model by D. S. Fisher [33].

We analyze the instabilities by varying randomly the relative orientation  $\theta$  between the two walls as well as the sliding direction  $\phi$ . At this point, we are only concerned with the occurrence of instabilities, rather than with the (average) amount of energy dissipated during an instability. Instabilities between incommensurate walls are shown in Fig. 1.

Unless  $\theta$  is close to an integer multiple of  $60^\circ$ , we find that the number of instabilities depends only weakly on  $\theta$  and  $\phi$ . If we chose the fundamental harmonics  $\tilde{V}(\mathbf{g})$  of both walls to be identical and the higher harmonics to be absent, then we find on average one instability each time the upper wall has been moved laterally with respect to the lower wall by a distance of  $200 d_{nn}$ . Increasing the interaction strength for just one wall does not change the behavior until the ratio  $\tilde{V}_t(\mathbf{g})/\tilde{V}_b(\mathbf{g})$  or its inverse exceeds about 4.7. Above this threshold value, the metastable positions and hence the particles follow the motion of just one wall and no instability occurs.

Like Daly *et al.* [24], we note that the instabilities are possible due to transverse motion of the impurities, see also Fig. 1. One of the issues Daly *et al.* also discussed was the question above which value of  $\tilde{V}_t(\mathbf{g})/\tilde{V}_b(\mathbf{g})$  the lubricant particle remains pinned to the (top) wall. They reported a value of 4.5, while we find a slightly higher value of 4.7, which essentially confirms the prediction. Furthermore, we also analyzed the effects of first higher harmonics, which were neglected in Ref. 24. Including the first higher harmonic  $\mathbf{g}_1$  in addition to the fundamental harmonics  $\mathbf{g}_0$  increases the number of instabilities, in particular for higher harmonics with positive sign. Thus, the occurrence of instability remains a robust feature of incommensurate walls. For a ratio  $V(\mathbf{g}_1)/V(\mathbf{g}_0) = 0.1$ , the number of instabilities is increased by a factor of six. (At this ratio the absolute value of the second harmonic would be in the order of  $0.01 V(\mathbf{g}_0)$ , see Eq. (17), and will thus be neglected.) One may argue that the observed increase in pops is related to an increase of incommensurability due to an additional (small) length scale.

### C. 3D Model

#### 1. Effect of commensurability on PDs

We now turn to the analysis of the full three-dimensional model, described in detail in Sect. III. Here, we also include the interaction between the lubricant atoms. However, as the coverage is only a quarter layer, the results remain almost identical to the ideal impurity limit. Despite these changes with respect to Section IV B, all arguments discussed there remain valid under the new conditions. For instance, Fig. 3 shows the expected dynamical behavior of two *commensurate* walls separated by lubricant impurities in sliding motion, i.e., an alteration of hcp and fcc type configurations. Most importantly, the trajectories of lubricant atoms become continuous for commensurate walls. It is instructive to compare Figs. 1 and 3. For completeness, we mention that the simulations in Figs. 1 and 3 were both done at an external load of  $L = 30$  per top wall atom, a thermal energy of  $T = 0.01$ , and relative sliding velocity of  $v_0 = 10^{-3}$ .

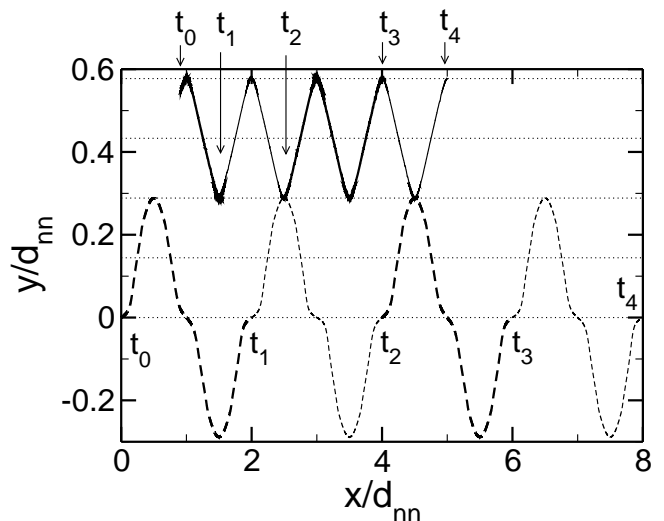


FIG. 3: Trajectory of a tagged particle (solid line) and of the upper wall (dashed line) for a commensurate system. The upper wall is moved parallel to  $x$  at constant velocity. Horizontal lines are drawn at intervals  $1/4\sqrt{3}$ . For integer values of  $x/d_{nn}$  the configurations can be identified as hcp, for half-integer values as fcc configurations.

The different trajectories of the mechanically stable states result in qualitatively different velocity distributions, even in the presence of thermal fluctuations, which is shown in Fig. 4. It can be seen that the velocity PDs of impurities between incommensurate walls can indeed be described with the non-equilibrium PD suggested in Eq. (9). It turns out that the PDs longitudinal ( $x$ ) and transverse ( $y$ ) to the sliding direction ( $x$ ) are almost identical. We note in passing that the velocity PD normal to the interface ( $z$  direction) is affected much less than the



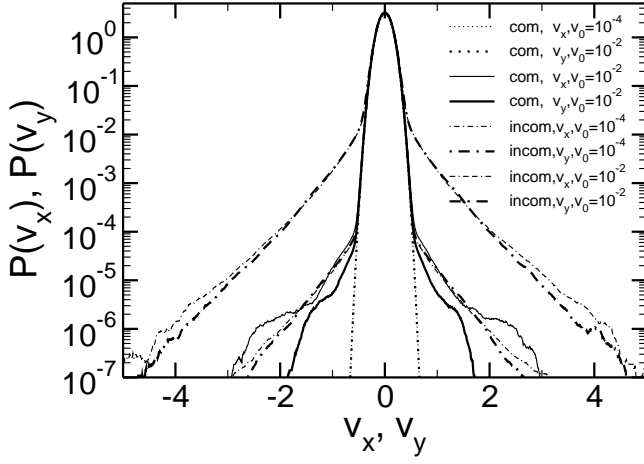


FIG. 4: Probability distribution (PD) of the fluid particles'  $x$ - and  $y$ -velocity components for shearing velocities  $v_0 = 10^{-4}$  and  $10^{-2}$  for incommensurate and commensurate wall orientations at  $T = 10^{-2}$  and  $L = 30$  for our standard system. Around the central Maxwell-Boltzmann PD wide tails develop upon shearing. The tails follow an exponential PD, see Eq. (9), which have similar magnitude parallel and transversal to the sliding direction. For commensurate walls, the tails are suppressed by two orders of magnitude at  $v_0 = 10^{-2}$  and disappear completely for the lower shear velocity  $v_0 = 10^{-4}$ , when the PDs becomes almost indistinguishable from the Maxwell PD (not included).

in-plane PDs.

### 2. Effect of sliding velocity and temperature on PDs

As the relative sliding velocity between the walls is changed by a factor of 100, the prefactor of the exponential tail scales with the same factor, as suggested in Eq. (9). The commensurate walls behave differently. First, the non-equilibrium velocity distribution  $P(v)$  deviates from equilibrium much less than for incommensurate walls and it does not obey Eq. (9) as well. More importantly, the tails of  $P(v)$  behave differently from those of incommensurate surfaces under a change of sliding velocity. This difference is due to the absence of instabilities for the commensurate system. At  $v_0 = 10^{-4}$ , the velocity PD for commensurate walls is almost identical to the equilibrium Maxwell Boltzmann PD, while at the same  $v_0$ , the PDs for incommensurate walls show distinct non-equilibrium tails. We employ a logarithmic scale for the PDs, because the tails can hardly be discerned on a linear scale.

Further examination of the distribution functions for incommensurate surfaces as shown in Fig. 5 reveals that the coefficients  $A$  and  $B$  in Eq. (11) are approximately constant for a wide range of velocities and temperatures. The parameters can be easily read off the graphs: The slope of the tails equals  $B$  and the exponential of the  $y$ -axis intercept of a fitted line through the tails equals  $Av_0$ .

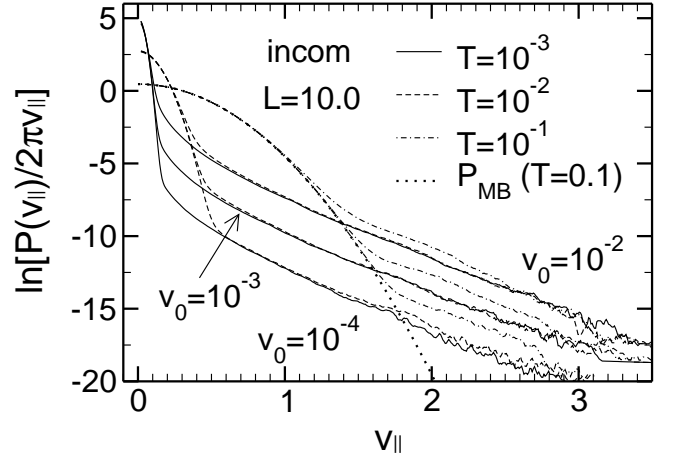


FIG. 5: Probability distribution  $\ln [P(v_{||})/2\pi v_{||}]$  at load  $L = 10.0$  for temperatures  $T = 10^{-3}$ ,  $T = 10^{-2}$ ,  $T = 10^{-1}$  and sliding speeds  $v_0 = 10^{-3}$ ,  $v_0 = 10^{-2}$ , and  $v_0 = 10^{-1}$ . At low in-plane velocities  $v_{||}$  a thermal peak described by the Maxwell-Boltzmann PD (at  $T = 0.1$  exemplified by a thick dotted line) dominates, before the PD crosses over to exponentially distributed tails described in Eq. (11). The slope of the tails,  $B$ , is independent of both  $T$  and  $v_0$ . The prefactor of the tail distribution is proportional to  $v_0$  and changes at large temperatures.

The data for Fig. 5 were produced with load  $L = 10.0$  for temperatures  $T = 10^{-3} \dots 10^{-1}$  and sliding speeds  $v_0 = 10^{-3} \dots 10^{-1}$ .

The present discussion is valid when the non-equilibrium tails are clearly visible such as in Fig. 5. It becomes invalid when  $v_0$  reaches extremely small values, i.e., when the tails are starting to disappear under the central Maxwell-Boltzmann peak. Eq. (9) then ceases to be a good description of the PDs in that limit and Eqs. (9) through (12) are no longer applicable. However, the equation describing the heat-flow balance between thermostat and confined system, Eq. (6), is unaffected by this argument and remains valid even in the limit  $v_0 \rightarrow 0$ .

### 3. Effect of load on PDs

The load dependence of the coefficients  $A$  and  $B$  was investigated as well. We show the effect of load on the PDs for one of our model systems exemplarily in Fig. 6. Many similar calculations were done for other loads, coverages, and sliding velocities with similar results for incommensurate surfaces. In all cases, we found that  $A$  is roughly proportional to  $L^{-0.8}$ , while  $B$  is approximately proportional to  $L^{-0.4}$ .

From the normalization factor of the central equilibrium peak in Eq. (12), one may infer that the ratio  $A/B^2$  is a measure for the number of atoms far out of equilibrium and hence for the number of invoked instabilities. Given the proportionalities  $A \propto L^{-0.8}$  and  $B \propto L^{-0.4}$ ,

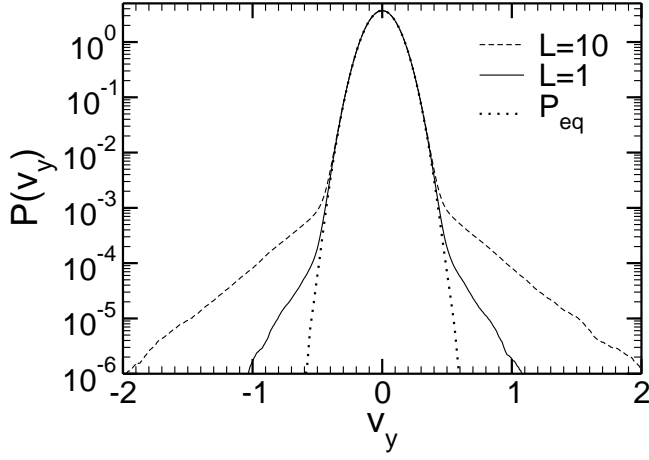


FIG. 6: Probability distribution  $P(v_y)$  at  $T = 0.01$ ,  $v_0 = 10^{-3}$  and two different loads  $L = 1.0$  and  $L = 10$ . The thermal equilibrium distribution  $P_{eq}$  is inserted for comparison.

this number remains constant when  $L$  is increased. Inserting the proportionalities  $A \propto L^{-0.8}$  and  $B \propto L^{-0.4}$  into Eq. (12) results in a small deviation from Amontons's law  $F_k \propto L$  at the microscopic level.

Potential differences scale with  $L$  in lowest order, thus we obtain for the energy dissipated in a pop  $\Delta E_{diss} \propto L \propto v^2$ . Hence, for exact proportionality, the width of the non-equilibrium tails was  $\propto L^{0.5}$ , respectively  $B \propto L^{-0.5}$ , yielding Amontons's law. This shows that  $B \propto L^{-\lambda}$ ,  $\lambda \approx 0.5$  is to be expected, while the precise value of the exponent  $\lambda$  will depend on the specific system potentials.

The deviation in our system is due to a shift of the relative significance of lower- and higher-order harmonics. This shift would presumably be smaller if the repulsive forces were modeled with (slightly more realistic) exponentially repulsive forces [37].

Fig. 6 reveals that the exponential tails fall off less slowly when the pressure is increased. Thus, large pressures in sliding contacts can dramatically increase the probability of large velocities, even though the lubricant's average kinetic energy  $\langle T_{kin} \rangle$  (or effective thermal energy) may barely change. This favours the occurrence of rare events such as chemical bond breaking, as it becomes much more likely that a bond is hit quasi-simultaneously by two high-velocity atoms. As the non-equilibrium PDs fall off less slowly than the equilibrium PDs, bond breaking will occur more frequently in non-equilibrium than in equilibrium at a given thermal energy  $\langle T_{kin} \rangle$ . It will thus be difficult to assign a unique effective temperature that reflects at the same time the reactivity of the molecules in the junction and the energy contained in the vibrations.

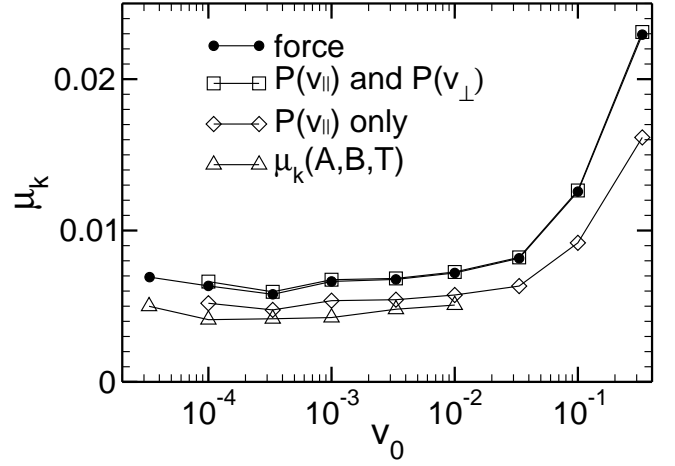


FIG. 7: Comparison between the friction coefficient  $\mu_k$  as measured directly at the wall and calculated indirectly through the non-equilibrium velocity distributions  $P(v)$ . In two cases, the true distributions  $P(v)$  were used. Taking into account both in-plane velocities  $v_{\parallel}$  and velocities  $v_{\perp}$  normal to the interface results in perfect agreement. We also first fitted the PDs to Eq. (11), determined the coefficients  $A$  and  $B$  from the simulations and then calculated the kinetic friction force with Eq. (12). Quarter layer of lubricant,  $T = 0.001$  and  $L = 30$ .

#### 4. Comparison between calculated and measured friction coefficients

The fit of curves equivalent to those shown in Figs. 4 and 5 allows one to estimate the kinetic friction force  $F_k$  with the help of Eq. (12). This result can then be compared to the friction force that is measured directly in the simulation. It turns out that such a comparison typically leads to an agreement within approximately 25 % accuracy, which can be improved by also taking into account the effects of instabilities on the motion normal to the surfaces. The deviation between the 'predicted'  $F_k$ 's and the directly measured  $F_k$ 's is due to the fact that the tails are not exactly exponential. This is particular important when the temperature is large or  $v_0$  extremely small. If we accumulate the correct  $P(v)$ 's in the simulation and use Eq. (6) to predict  $F_k$ , the agreement between predicted and observed kinetic friction is almost perfect, also when  $v_0$  tends to zero.

Fig. 7 shows the degree of agreement for one particular model system. One can see that the kinetic friction coefficients  $\mu_k$  as obtained from the full velocity PD, see Eqs. (6) and (7) agree perfectly quite well with the directly measured  $\mu_k$ . Neglecting the contribution of the motion normal to the surface results in an  $\mathcal{O}(20\%)$  underestimation of the friction force. Estimating  $\mu_k$  indirectly with the help of Eqs. (11) and (12) leads to an underestimation of about 25%.

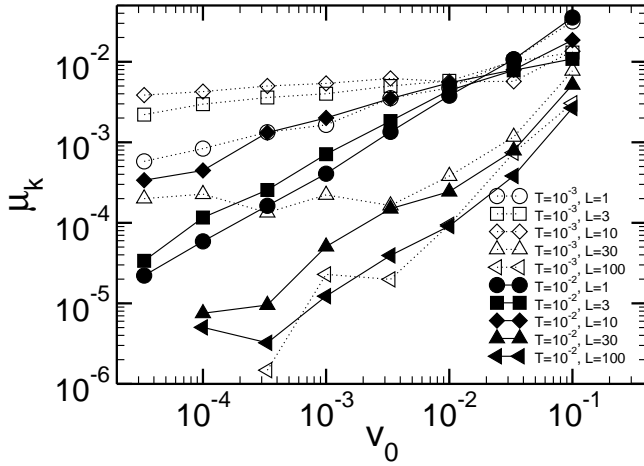


FIG. 8:  $\mu_k$  of the commensurate standard system versus pulling velocity  $v_0$  at different normal loads  $L$  and temperatures  $T$ . Note the logarithmic scale for the  $y$ -axis. In all cases  $\mu_k$  vanishes with a power law  $v^\beta$  as  $v \rightarrow 0$ , except for  $T = 10^{-3}$ ,  $L = 30$  where a constant, small value seems to be reached.

### 5. Effect of temperature

It was shown by He and Robbins [28] that the model system on which this study is based yields logarithmic velocity corrections to the friction force  $F_k$  for *incommensurate* surfaces, provided the temperature is positive and the sliding velocity is not too small, see also the discussion in Ref. [18]. Our simulation results of the  $v_0$  corrections to  $F_k$  for incommensurate surfaces are not shown explicitly, however, they confirm the results by He and Robbins. The basic reason for a logarithmic-type correction had already been recognized by Prandtl [8]. Due to thermal fluctuations, the embedded atoms can jump over local energy barriers and the instabilities will be ignited prematurely. This reduces the necessary external force to maintain sliding, because it does not need to move the embedded atom all the way to the top of the energy barrier.

For *commensurate* surfaces, discontinuous instabilities are absent and therefore the effect of thermal fluctuations must be different. This issue is investigated in Fig. 8. Due to the large loads and the small temperatures employed, the linear-response regime is not necessarily reached at the sliding velocities  $v_0$  accessible to the simulations, i.e.,  $v_0 = 10^{-5}$ . Therefore, we obtain kinetic friction coefficients  $\mu_k$  that apparently vanish according to

$$\mu_k \stackrel{v_0 \rightarrow 0}{\propto} v_0^\beta, \quad (18)$$

with exponents  $0.25 \lesssim \beta \lesssim 1$ .

It is remarkable that a small change in temperature has a rather strong effect on  $F_k$ . For the small load  $L = 1$ , the exponent  $\beta$  is approximately unity at temperature  $T = 10^{-2}$  and one may argue that the corresponding

$F_k(v_0)$  reflects a linear response curve. As  $T$  is lowered to  $T = 10^{-3}$ , a different exponent  $\beta$  is obtained, reflecting non-equilibrium behavior. When the load is now increased by a factor of ten, the energy barriers also increase approximately by a factor of ten. Therefore the  $F_k(v_0)$  curves belonging to masses  $L \gtrsim 10$  should be considered far from equilibrium, i.e. athermal. This would favour exponents  $\beta$  less than unity. However, this expectation is not true. Instead a Stokes-type friction is observed. The almost linear relation of  $F_k$  and  $v_0$  for these largest loads ( $L = 100$ ) may thus be an effect due to higher harmonics in the lubricant-wall potential. As one can see in the 1D, incommensurate systems, i.e., Fig. 2, the friction-velocity relationship can change qualitatively at certain critical values of the higher-order harmonics.

## V. BEYOND THE IMPURITY LIMIT

So far, we have neglected the *direct* interactions between the impurities or the coverages were small enough in order to render the direct interactions negligible. This approximation is reasonable when the coverage is small and when the lubricant particles are simple spherical units without inner degrees of freedom. When either condition is violated, the energy landscape and hence the detailed characteristics of the instabilities will change. This in turn might lead to a qualitative change in the tribological behavior of the junction. In this section, we will study the applicability, the limitations and corrections of the impurity limit model that are due to the interactions between lubricant atoms.

### A. Coverage effects

When the lubricant coverage is close to or greater than one monolayer and the junction is sheared, particles will have to move in a correlated fashion. In order for one atom to jump to another mechanically stable site, its neighbor has to jump as well, etc. A detailed description of the dynamics will be very complicated, i.e., it may involve sliding of correlated blocks along grain boundaries and the formation of dislocation-type structures [38]. Yet, the argument persists that instabilities and sliding induced deviations from the equilibrium velocity distribution function lead to friction.

Besides the correlated motion, some more details change when the coverage is increased. For example, pops also occur in the direction normal to the interface with a similar magnitude as parallel to the interface. This is reflected in the probability distributions  $P(v)$  for the in-plane velocity  $v_{\parallel} = \sqrt{v_x^2 + v_y^2}$  and the normal component  $v_{\perp} = v_z$  of the fluid particles, see Fig. 9. The system under consideration is incommensurate, the walls are separated by a double layer and the externally imposed load per wall atom is  $L = 30$ . Although the detailed

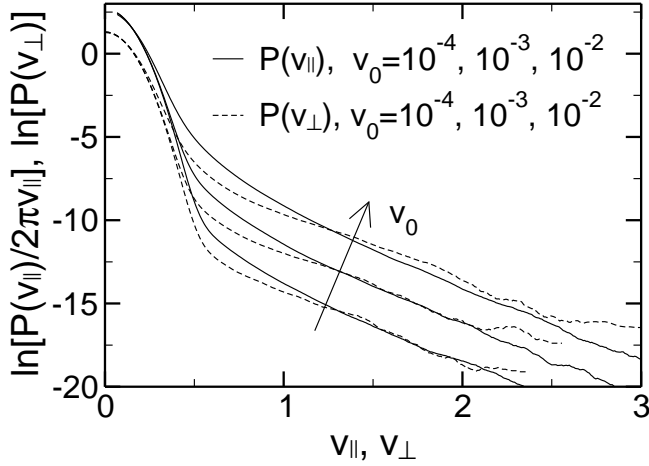


FIG. 9: Distribution of the fluid particles velocity in plane, ( $P(v_{\parallel})$ ), and perpendicular to it, ( $P(v_{\perp})$ ), for an incommensurate system with two monolayers coverage at sliding velocities  $v_0 = 10^{-4}$ ,  $10^{-3}$ , and  $10^{-2}$ . The central Maxwell-Boltzmann parts are shifted because of the normalization  $1/2\pi v_{\parallel}$  of  $P(v_{\parallel})$ .

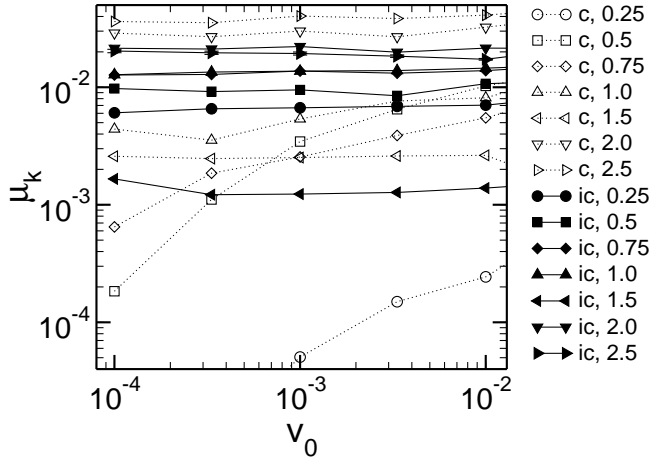


FIG. 10: Coverage dependence of the dynamic friction coefficient  $\mu_k$  of a system containing 0.25...2.5 monolayers of simple liquid at  $T = 10^{-2}$  and  $L = 30$ . Commensurate systems (c) are denoted with open symbols, incommensurate walls (ic) with full symbols.

dynamics of the lubricant atoms must be very different from those in the impurity limit, Eqs. (9) and (11) provide again a reasonable description for respectively  $P(v_{\perp})$  and  $P(v_{\parallel})$ , i.e., a central Maxwell-Boltzmann peak and a non-equilibrium exponential tail. Similar curves, which are not shown explicitly, were obtained for a coverage up to 5 monolayers.

As before, the kinetic friction force  $F_k$  is the integral over the deviation of the  $P(v)$ 's from the Maxwell-Boltzmann distribution, as stated in Eq. (6).  $F_k$  is shown for various coverages and sliding velocities in Fig. 10. Both commensurate and incommensurate systems are investigated and again their behavior is strikingly different.

We start our discussion with the commensurate system. At a coverage of  $C = 0.25$ , results are very close to the impurity limit.  $F_k$  decays to zero with a powerlaw  $v^{\beta}$  where the exponent  $\beta$  is less than one. As the coverage is increased to  $C = 0.5$  or even  $C = 0.75$ ,  $F_k$  decreases considerably less quickly with decreasing  $v_0$  than in the impurity limit. The behavior remains strikingly different from Coulomb friction. This changes when the coverage reaches and exceeds one full monolayer. For coverages beyond double layers, the kinetic friction force even exceeds that of incommensurate systems. The prediction in Ref. 18 that commensurate systems should show smaller kinetic friction than incommensurate system must thus be limited to extreme boundary lubrication. Above one monolayer lubrication, this trends seemingly turns around. Experiments suggest that commensurability leads to enhanced friction between mica surfaces lubricated by a double layer or more [39]. Unfortunately, no study is known to the authors in which a monolayer of lubrication or less was used between two (smoothly) sliding commensurate walls.

At the smallest velocity investigated,  $\mu_k$  increases by a factor greater than 200 for the *commensurate* case, when we increase the coverage from  $C = 0.5$  to  $C = 2$ . The same change in coverage for incommensurate surfaces only yields a factor of two. Hence, incommensurate surfaces show much weaker coverage dependence than commensurate interfaces. Overall, there is relatively little change of  $F_k$  with coverage for incommensurate walls with the exception of  $C = 1.5$ . Due to the large load employed, the 1.5 monolayers are squeezed into a single layer, which then essentially acts like a solid. This situation would not occur - or at least occur only for a short period of time - if the lubricant could flow out of the junction. We conclude that the coverage dependence is weak for incommensurate walls.

## B. Effects due to molecular bonds

Most lubricant particles possess an inner structure. Here we will focus on the most simple generalization of the spherical molecules considered so far, namely dimers, and hexamers (6-mers). Dimers would represent small linear molecules such as  $C_2H_6$ , while hexamers are representative of short, linear alkane chains. The dynamics of the lubricant particles will change due to the additional internal degrees of freedom. Alternatively, one may argue that the dynamics of monomers is restricted because every monomer is constraint by at least one chemically bonded neighbor.

While monomers only have translational degrees of freedom, dimers also have *rotational* degrees of freedom. It is tempting to speculate that 'rotational' instabilities can occur in addition to the 'translational' instabilities. Therefore, one might expect  $F_k$  to be larger for dimers than for monomers. However, the rotational and translation motion will not be independent of each other and

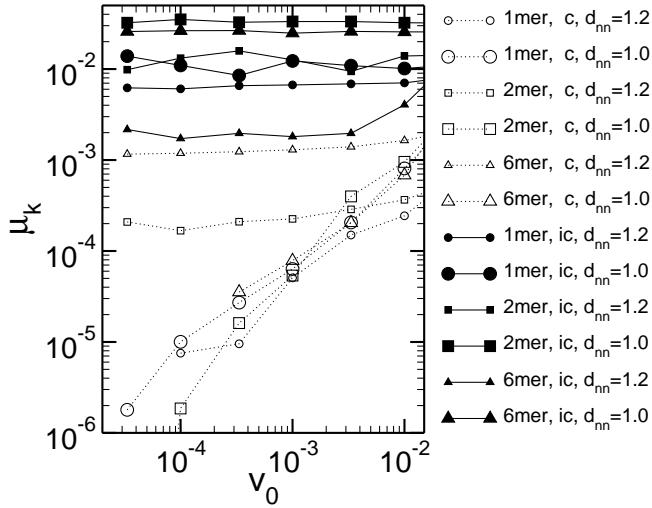


FIG. 11: Dependence of the friction coefficient  $\mu_k$  on the wall lattice constant  $d_{nn}$  for a quarter monolayer of a dimer and a 6-mer with bond-length  $d_{mol} = 0.967$  for commensurate (c, open symbols) and incommensurate (ic, full symbols) orientation at small temperatures  $T = 10^{-2}$  and large loads  $L \approx 30$  (adjusted to yield identical pressures).

the coupling between them might reduce the effect of a 'translational' instability. The question which effect dominates can only be answered by analytical calculations or by molecular dynamics simulations. Simulation results for the kinetic friction force in a boundary-lubricated interface are shown in Fig. 11.

In Fig. 11, one can learn that the ratio  $\rho = d_{nn}/d_{mol}$  of the next neighbor spacing  $d_{nn}$  in the walls and the intra-molecular bond length  $d_{mol}$  plays an important role, particularly for commensurate surfaces. When the intra-molecular bond length is close to the next-neighbor distance of wall atoms  $d_{nn}$ ,  $F_k$  disappears as a power law with sliding velocity  $v_0$ . This means that the 'interference' effects between commensurate walls persist and that no instabilities occur. Surprisingly, this is even observed for hexamers. However, if  $d_{mol}$  differs from  $d_{nn}$ , instabilities also occur in boundary-lubricated systems, even for commensurate walls. These instabilities are invoked through the rotational degrees of freedom. While the misfit between  $d_{mol}$  and  $d_{nn}$  leads to Coulomb friction between commensurate walls, its value of  $F_k$  remains small as compared to the incommensurate case.

We now turn to the incommensurate walls. Interestingly, the smoother walls with  $d_{nn} = 1.0$  produce higher kinetic friction than the walls with  $d_{nn} = 1.2$ , while the opposite is true for obvious reasons in the case of static friction  $F_s$ . The reason for the effect in  $F_k$  is that the reduced nearest neighbor spacing leads to a higher rate of popping processes, as more atoms sliding past each other at a given  $v_0$  while the energy gain in the pops is only slightly decreasing. This effect can be verified by comparing the distributions of the particle velocities. The effect remains stable for all degrees of polymerization. The

high friction of a dimer is caused by the contribution of their fast rotations. This is revealed by the distribution of the bonds' angular velocities. Despite these trends, incommensurate systems prove again to be less susceptible to quantitative changes in the parameters that determine the details of the model than commensurate systems.

## VI. CONCLUSIONS

Kinetic friction requires the prevalence of instabilities (mechanical hysteresis) in a system. In the present paper, we have focused on instabilities in the trajectories of particles confined between two walls, which are sheared against each other. When an instability is reached, the particle does not find a local potential energy minimum in its vicinity anymore and is thus forced to "pop" into the next local minimum it sees. At small sliding velocity  $v_0$ , this will lead to a high velocity, which depends solely on the energy landscape. The kinetic energy is gradually dissipated, resulting in a frictional force. We derived a relationship between the (non-equilibrium) velocity distribution function  $P(v)$  and the friction force  $F_k$ . The characteristics of  $P(v)$  and thus  $F_k$  depend only weakly on coverage, sliding velocity, load and other parameters for incommensurate surfaces.

In a generic setup, we first used two Steele potentials reflecting two two-dimensional, triangular walls, which could be rotated with respect to each other to achieve an incommensurate system. We then computed numerically the adiabatic trajectory of a test particle. It was found that instabilities were a robust feature of the incommensurate system. Different off-symmetry wall rotations and inclusion of higher-order contributions to the Steele potential as well as asymmetric interaction strengths of the walls did not alter the occurrence of the instabilities, but only affected their frequency.

Including interactions between lubricant atoms does not change the existence of instabilities and hence the presence of Coulomb friction either. In contrast, the commensurability of the walls allowed for especially smooth trajectories of impurity atoms. The trajectories remain smooth when interactions between lubricant atoms are included up to a coverage of one monolayer. Above one monolayer, the lubricant atoms do not move coherently any longer and instabilities are starting to occur within the film. Kinetic friction rises dramatically as a consequence.

We speculate that coherent motion similar to the one just described may also be responsible for the behavior observed in a pioneering quartz crystal oscillator study by Krim and Chiarello [40]. They found that the friction between a *solid* monolayer and a smooth surface was much smaller than the friction between a fluid monolayer and the same surface. The reverse was reported for a rough surface. Of course, the motion of a layer adsorbed on a microbalance is different from that of a "between"-sorbed layer, because in the first case, there is no confining top

wall and sliding-induced wall interference effects cannot occur. This is an important qualitative difference, which prevents us from making a direct comparison of our simulations with the above-mentioned experiments. One may yet argue that commensurability can induce coherent motion of the film, be it adsorbed or "between"-sorbed. This suppresses erratic pops, which ultimately lead to energy dissipation. Thus, if one assumes that film and smooth substrate were commensurate, the small values for the kinetic friction force would not necessarily be in contradiction to the supposedly large static friction force. On the other hand for rough, disordered surfaces, a solid monolayer would not be able to move coherently, which would be consistent with its large friction as compared to a fluid layer.

We turn back to the discussion of the non-equilibrium velocity distributions. For incommensurate walls, the distribution consists of a central peak, which is essentially identical to the equilibrium velocity distribution, and of an additional non-equilibrium tails. These tails fall off only exponentially with  $v$ , which is slower than the exponential decay with  $v^2$  in equilibrium systems. This observation is rather generic for incommensurate systems and independent of the lubricant coverage. As the real velocity distribution function is qualitatively different from Gaussians, it seems futile to describe the interface in terms of an effective temperature. We argued that given a specific kinetic energy associated with a lubricant (which could be used to define an effective temperature), the non-equilibrium system would be more likely to invoke chemical bond breaking or other chemical reactions.

Overall, the impurity model provides a good description of the typical characteristics of a boundary-lubricated system. However, it is essential to study

two-dimensional interfaces and incommensurate surfaces. One-dimensional and/or commensurate surfaces lead to untypical behavior, i.e., rather large sensitivity of the friction force with respect to small changes in the model (details of interaction potential) or in the external parameters (sliding velocity, load, temperature, etc.). This is unfortunate, because incommensurate walls are much more common than commensurate walls, which leaves us with fewer possibilities to control friction.

A surprising result of our study for incommensurate walls is that increasing the atomic scale roughness of the walls may actually sometimes reduce the kinetic friction force.

It would be interesting to compare our predictions concerning the velocity distributions to experimental data. While scattering data from small, confined volumes is certainly notoriously difficult to obtain, recent advances have been made. Using fluorescence correlation spectroscopy, Mukhopadhyay et. al. [41] measured translational diffusion in molecularly thin liquids confined within a surface forces apparatus. In the future, it might be possible to extend these studies to sliding situations so that velocity distributions can be measured.

#### Acknowledgments

M.A. is indebted to J. Baschnagel and M. Fuchs for numerous discussions and acknowledges support by the German Academic Exchange Service (DAAD, "Hochschulsonderprogramm III von Bund und Ländern"), grant no. D/00/07994. We are also grateful to the Bundesministerium für Bildung und Forschung (BMBF) for partial support under grants no. D.I.P. 352-101 and 03N6500.

- 
- [1] B. N. J. Persson, *Sliding Friction: Physical Principles and Applications* (Springer, Berlin, 1998).
  - [2] B. Bhushan, *Principles and Applications of Tribology* (Wiley, New York, 1999).
  - [3] D. Dowson, *History of Tribology* (Longman, New York, 1979).
  - [4] M. Brillouin, *Notices sur les Travaux Scientifiques* (Gauthiers-Vilars, Paris, 1909).
  - [5] C. Caroli and P. Nozières, *Eur. Phys. J. B* **4**, 233 (1998).
  - [6] M. H. Müser, M. Urbakh, and M. O. Robbins, *Adv. Chem. Phys.* **126**, 187 (2003).
  - [7] E. Gnecco, R. Bennewitz, and E. Meyer, *Phys. Rev. Lett.* **88**, 215501 (2002).
  - [8] L. Prandtl, *ZS. f. angew. Math. u. Mech.* **8**, 85 (1928).
  - [9] G. A. Tomlinson, *Phil. Mag. Series* **7**, 905 (1929).
  - [10] Y. I. Frenkel and T. Kontorova, *Zh. Eksp. Teor. Fiz.* **8**, 1340 (1938).
  - [11] O. M. Braun and Y. S. Kivshar, *Phys. Rep.* **306**, 1 (1998).
  - [12] M. G. Rozman, M. Urbakh, and J. Klafter, *Phys. Rev. Lett.* **77**, 683 (1996).
  - [13] M. G. Rozman, M. Urbakh, and J. Klafter, *Phys. Rev. E* **54**, 6485 (1996).
  - [14] P. A. Thompson and M. O. Robbins, *Science* **250**, 792 (1990).
  - [15] P. A. Thompson and M. O. Robbins, *Phys. Rev. A* **41**, 6830 (1990).
  - [16] L. Wenning and M. H. Müser, *Europhys. Lett.* **54**, 693 (2001).
  - [17] B. N. J. Persson, V. N. Samoilov, S. Zilberman, and A. Nitzan, *J. Chem. Phys.* **117**, 3897 (2002).
  - [18] M. H. Müser, *Phys. Rev. Lett.* **126**, 224301 (2002).
  - [19] H. Risken, *The Fokker Planck equation* (Springer, Heidelberg, 1984).
  - [20] O. M. Braun and M. Peyrard, *Phys. Rev. E* **63**, 046110 (2001).
  - [21] P. Espanol and P. Warren, *Europhys. Lett.* **30**, 191 (1995).
  - [22] H. Mori, *Prog. Theor. Phys.* **33**, 7526 (1965).
  - [23] R. Zwanzig, *Annu. Rev. Phys. Chem.* **16**, 67 (1965).
  - [24] C. Daly, J. Zhang, and J. B. Sokoloff, *cond-mat/0208393* (2002).
  - [25] E. Jaynes, *Papers on Probability, Statistics and Statisti-*

cal Physics (Reidel, Dordrecht, 1982).

- [26] J. Honerkamp, *Statistical Physics* (Springer, Berlin, 1998), chap. 2.5.
- [27] The projection  $P(v_x) = \int P(v_x, v_y) dv_y = \int \exp[-B\sqrt{v_x^2 + v_y^2}] dv_y$  is in general only approximately exponential. However, for sufficiently large  $v_x$ , this approximation is very accurate and  $B'$  with  $\exp[-B'v_x] \simeq P(v_x)$  is close to  $B$ .
- [28] G. He and M. O. Robbins, *Tribol. Lett.* **10**, 7 (2001).
- [29] K. S. und M. Hirano, *Surf. Sci.* **283**, 473 (1993).
- [30] K. Kremer and G. S. Grest, *J. Chem. Phys.* **92**, 5057 (1990).
- [31] J. M. Haile, *Molecular Dynamics Simulation: Elementary Methods* (John Wiley and Sons, Inc., New York, 1997).
- [32] M. P. Allen and D. J. Tildesley, *Computer Simulation of Liquids* (Oxford Science Publications, Oxford, 1987).
- [33] D. S. Fisher, *Phys. Rev B* **31**, 1396 (1985).
- [34] W. Steele, *Surface Science* **36**, 317 (1973).
- [35] A. Patrykiewicz, S. Sokołowski, and K. Binder, *Surface Science Reports* **37**(6-8), 207 (2000).
- [36] Wolfram Research, Inc., *FindMinimum[ ] in Mathematica (R), Version 4.1.0.0 for Linux*.
- [37] M. H. Müser, L. Wenning, and M. O. Robbins, *Phys. Rev. Lett.* **86**, 1295 (2001).
- [38] B. N. J. Persson and P. Ballone, *J. Chem. Phys.* **112**, 9524 (2000).
- [39] M. Ruths and S. Granick, *Langmuir* **16**, 8368 (2000).
- [40] J. Krim and R. Chiarello, *J. Vac. Sci. Technol. B* **9**, 1343 (1991).
- [41] A. Mukhopadhyay, J. Zhao, S. C. Bae, and S. Granick, *Phys. Rev. Lett.* **89**, 136103 (2002).

## APPENDIX A: RELATION BETWEEN VELOCITY DISTRIBUTION AND FRICTION

Consider a system in steady-state equilibrium with the following underlying equation of motion

$$m\ddot{\mathbf{x}} + m\gamma\dot{\mathbf{x}} = \mathbf{F}_b(\mathbf{x}) + \mathbf{F}_t(\mathbf{x} - \mathbf{v}_0 t) + \mathbf{\Gamma}(t). \quad (\text{A1})$$

Here, we chose the same terminology as in Sect. II, i.e.,  $\mathbf{F}_b(\mathbf{x})$  denotes the force of the bottom wall on an impurity atom located at position  $\mathbf{x}$  and  $\mathbf{v}_0$  is the velocity of the upper wall with respect to the substrate. We multiply Eq. (A1) with  $\dot{\mathbf{x}}$  and average over a long time interval  $\tau$ . We then interpret the resulting individual terms. They can be associated with the (average) power dissipated within the system or the (average) power put into the system. First, the average change of kinetic energy with time equals zero, namely

$$\begin{aligned} \frac{1}{\tau} \int_0^\tau dt m\ddot{\mathbf{x}}\dot{\mathbf{x}} &= \frac{1}{\tau} \int_0^\tau dt \frac{d}{dt} T_{\text{kin}} \\ &= \frac{1}{\tau} [T_{\text{kin}}(t = \tau) - T_{\text{kin}}(t = 0)] \\ &\rightarrow 0 \text{ for } \tau \rightarrow \infty \end{aligned} \quad (\text{A2})$$

The second term is proportional to the time-averaged kinetic energy of the system with respect to the lower

wall:

$$\begin{aligned} \frac{1}{\tau} \int_0^\tau dt m\gamma\dot{\mathbf{x}}\dot{\mathbf{x}} &= \gamma m \langle \dot{\mathbf{x}}^2 \rangle \\ &= 2\gamma \langle T_{\text{kin}} \rangle, \end{aligned} \quad (\text{A3})$$

$\langle T_{\text{kin}} \rangle$  being the time-averaged or ensemble-averaged (steady-state) kinetic energy of an impurity. Thermostating also parallel to the top wall, e.g. by choosing  $\gamma = \gamma_t = \gamma_b$ , requires a trivial modification of the reference system. The next term is the average work of the bottom wall on the impurity

$$\begin{aligned} \frac{1}{\tau} \int_0^\tau dt \dot{\mathbf{x}} \mathbf{F}_b(\mathbf{x}) &= \frac{1}{\tau} \int_0^\tau dt \left( -\frac{d}{dt} V_b(\mathbf{x}) \right) \\ &= \frac{1}{\tau} \{V_b[\mathbf{x}(\tau)] - V_b[\mathbf{x}(0)]\} \\ &\rightarrow 0, \end{aligned} \quad (\text{A4})$$

which must vanish in any steady-state system. Of course, if the model was generalized such that (steady state) wear would occur, then the contribution discussed in Eq. (A4) would indeed remain finite.

For the discussion of the next term in Eq. (A1), it is necessary to keep in mind that

$$\frac{d}{dt} V_t(\mathbf{x} - \mathbf{v}_0 t) = -F_t(\mathbf{x} - \mathbf{v}_0 t) [\dot{\mathbf{x}} - \mathbf{v}_0]. \quad (\text{A5})$$

This and the same considerations invoked for Eq. (A4) yield

$$\frac{1}{\tau} \int_0^\tau dt \dot{\mathbf{x}} \mathbf{F}_t(\mathbf{x} - \mathbf{v}_0 t) = \langle \mathbf{F}_t \rangle \mathbf{v}_0, \quad (\text{A6})$$

where  $\langle \mathbf{F}_t \rangle$  is the time- or ensemble-averaged force that the top wall exerts on an impurity. This force or depending on the definition its projection onto the sliding direction can be associated with the kinetic friction force  $F_k$ .

The contribution due to the random force  $\mathbf{\Gamma}(t)$  is the most difficult contribution to calculate. However, if the system is close to local equilibrium for most of the time, then the expectation value of  $\mathbf{\Gamma}(t)\dot{\mathbf{x}}$  can be expected to be close to the value of this expression in thermal equilibrium. In equilibrium, it must compensate the expression discussed in Eq. (A3), hence

$$\frac{1}{\tau} \int_0^\tau dt \dot{\mathbf{x}} \mathbf{\Gamma}(t) \approx 2\gamma \langle T_{\text{kin}} \rangle_{\text{eq}}, \quad (\text{A7})$$

where  $\langle T_{\text{kin}} \rangle_{\text{eq}}$  denotes the average kinetic energy in thermal equilibrium.

Assembling all necessary terms, yields

$$2\gamma(\langle T_{\text{kin}} \rangle - \langle T_{\text{kin}} \rangle_{\text{eq}}) = F_k v_0. \quad (\text{A8})$$

Note that Eq. (A8) is equivalent to Eqs. (6) and (7).